Single-electron tunneling in nanometer-scale double-barrier heterostructure devices

Bo Su and V. J. Goldman
Department of Physics, State University of New York, Stony Brook, New York 11794-3800

J. E. Cunningham
AT&T Bell Laboratories, Holmdel, New Jersey 07733
(Received 10 March 1992)

We report a systematic experimental study of charge transport in nanometer-scale double-barrier resonant-tunneling devices. Asymmetric heterostructure material was used so that one barrier is substantially less transparent than the other. Resonant tunneling through size-quantized well states and single-electron charging of the well are thus largely separated in the two bias polarities. When the emitter barrier is more transparent than the collector barrier, electrons accumulate in the well; incremental electron occupation of the well, *starting from zero,* is accompanied by Coulomb blockade, which leads to sharp steps of the tunneling current. The voltage extent of the steps is affected by the intrawell electron-electron interaction. When the emitter barrier is less transparent, the current reflects resonant tunneling of just one electron at a time through size-quantized well states; the current peaks and/or steps (depending on experimental parameters) appear in current-voltage characteristics. Experimental results on magnetic field and temperature dependence of the current-voltage curves are also reported. Good agreement is achieved in comparison of many features of the experimental data with simple theoretical models.

I. INTRODUCTION

Charge transport by tunneling in semiconductor microstructures has attracted considerable attention, both experimental[1-11] and theoretical,[12-20] in recent years. Three-dimensional (3D) confinement is achieved either by vertical etching (quantum dots) of double-barrier resonant-tunneling structures (DBRTS),[1-7] or by lateral gating of 2D electron layer in heterojunctions (Coulomb islands).[8-11] Although, in principle, both quantum dots and Coulomb islands are 3D-confined volumes connected to two Fermi reservoirs in the electrodes through two penetrable barriers, there are several differences in experimentally realizable devices. While single-electron charging is dominant in Coulomb islands (the charging energy $U_C \gg \delta E$, separation of the single-particle energy levels in the confining potential),[8-11] size quantization and single-electron charging can be of the same order in quantum dots.[6,7] The transmission coefficient of a gate-induced barrier is adjustable, but not known; in DBRTS's, the tunneling barriers are well characterized and can be made in an extremely wide range of parameters. In DBRTS nanometer-scale devices, both energy and the in-plane angular momentum are conserved in tunneling; in the lateral tunneling in Coulomb islands, only energy is conserved.

A Coulomb island usually contains a relatively large number (70 to 1000) of electrons,[8-11] depending on its size, and, consequently, the charging energy U_C for adding one extra electron is nearly independent of the total number of electrons in the island. Because gate-induced barriers are low and wide, charging of a Coulomb island is usually achieved by a gate and the number of electrons in the island deviates from the equilibrium value at most by one. In the DBRTS quantum dots, at zero bias there are no electrons in the well. DBRTS's are difficult (but possible[4]) to gate and the well is populated by applying a large bias across the barriers. Thus the total number of electrons in the dot increases with bias in increments of one starting from zero, and all electrons are "extra"; the charging energy for adding the first electron (U_{1e}) is much different from that needed to add the second electron (U_{2e}) and the energy for the second electron is different from that for the third.[6,7] This is, in part, because the intrawell electron-electron interaction energy per electron depends on the total number of electrons in the dot and, in part, because of the different spatial extent of electronic charge distribution for different size-quantized states in the well.[6,7,21,22]

We have previously reported the observation of single-electron charging in nanometer-scale DBRTS devices.[6,7] We studied asymmetric DBRTS nanometer-scale devices and thus we were able to separate most of the single-electron charging effects from those due to size quantization. In this paper, we present a systematic experimental study of the tunneling charge transport in these devices. In Sec. II we describe fabrication and measurement details. In Sec. III we briefly review transport and charging of the well in large-area devices.[23] In Sec. IV we present our results on transport in nanometer devices at zero magnetic field and low temperature. Magnetotunneling study is given in Sec. V. Temperature dependence of the current-voltage curves is the subject of Sec. VI.

II. SAMPLES AND EXPERIMENT

Our DBRTS material was grown by molecular-beam epitaxy. The active layer consists of a 9-nm GaAs well sandwiched between a 10-nm $Al_{0.34}Ga_{0.66}As$ barrier and an 11.5-nm $Al_{0.36}Ga_{0.64}As$ barrier (substrate side). The

GaAs emitter and collector electrodes are Si doped to 2×10^{17} cm^{-3}; nominally undoped spacers of 10 and 8 nm are inserted before and after, respectively, the double-barrier region in order to limit Si concentration in the well. The wafer has a 100-nm-thick nonalloyed Al Ohmic contact grown *in situ* so that no heat treatment of the devices was needed. The double-barrier region is ~300 nm below the surface of the wafer.

Devices of nominal diameter $D=0.5$ to 3 μm were defined by electron-beam lithography and wet chemical etching as described below. As discussed elsewhere,[5] the electrical size of devices a is smaller than D by ~350 nm because of etching undercut and surface depletion. After polymethylmethacrylate (PMMA) coating of ~200 nm, wafers were baked at 125 °C for 90 min. The next step is the electron-beam writing of the area to be etched away; unexposed areas define devices so that possible electron-bombardment damage of the GaAs material is minimized. After developing, the exposed Al layer is removed by etching in diluted HCl and thus exposed heterostructure material is processed with a GaAs etchant of about 10 nm/s etching rate. The total mesa height is typically 350 nm; the top Al Ohmic contacts of the devices are contacted by In bonding pads vacuum evaporated at 45° (pads are 100×300 μm, defined by a lift-off lithography).

Measurements were done in a top-loading dilution refrigerator with both sample and thermometer immersed in the mixture. Temperature was measured by a calibrated Ru_2O_3 chip resistor mounted close to the sample. The current-voltage (I-V) curves of the devices were measured using a very-low-noise voltage-source biasing circuit. Derivatives were obtained by numerical differentiation.

III. LARGE-AREA DEVICES

In large-area DBRTS devices with barriers thicker than ~2 nm, resonant tunneling is incoherent; electrons first tunnel from the emitter electrode into 2D resonant states in the well; subsequently, electrons leave the well by tunneling through the collector barrier.[24] The tunneling electrons are dynamically stored in the well, creating a space-charge layer which can strongly affect relative energy alignment of the well with respect to the emitter.[23] The number of electrons in the well N_W is proportional to the tunneling current I, $N_W=I\tau_W/e$, where τ_W is the electron lifetime in the well (both I and N_W are proportional to the area of the device). Since I is, in turn, determined by the relative energy alignment of the well and emitter, this feedback mechanism can lead to intrinsic bistability of a device instead of negative differential conductance.[23]

As has been shown in Ref. 23, large-area DBRTS devices contain $n_W\sim10^{10}$ cm^{-2} electrons in the well near current threshold; therefore it was expected that a submicrometer DBRTS device with "electrical diameter" of $\sim10^{-5}$ cm would have just one electron in the well. In such devices, it was expected, tunneling of a single electron can result in appreciable charging of the well so that the probability of tunneling of the next electron is drastically affected and tunneling of individual electrons would be correlated in a manner similar to that in metal double junctions.[25,26]

The band diagrams of a large-area device under positive and negative bias are shown in Fig. 1. The Fermi energy E_F in the electrodes is about 20 meV; the energy of the bottom of the resonant 2D subband in the well $E_0\approx40$ meV. The energy separation between μ_E in the emitter and E_0 is denoted as ΔE. ΔE is negative at zero bias; as bias is increased, no resonant tunneling is possible until $\Delta E=0$ at threshold voltage $V_{\rm th}$. As bias is increased further, tunneling current increases until $\Delta E\approx E_F$, after that energy- *and* transverse-momentum-conserving resonant tunneling is no longer possible and current drops. Under positive bias, the emitter barrier is less transparent than the collector barrier, $T_E\ll T_C$, where T_E and T_C are transmission coefficients (generally, bias dependent). Therefore areal electron density in the well n_W is relatively small and the resulting space-charge layer affects ΔE little. Under negative bias, $T_E\gg T_C$ and n_W is quite considerable (typically, $1-5\times10^{11}$ cm^{-2} near peak current); the resulting negative feedback reduces ΔE for a given bias, thus shifting the peak of the tunneling current to higher (in magnitude) bias and causing bistability of I-V characteristic. We determine the voltage dependences $n_W(V)$, $T_E(V)$, $T_C(V)$, and others for both bias polarities by fitting experimental data of a large-area device with a generalization of the self-consistent DBRTS model described in Ref. 23.

Figure 2 shows the I-V curve of a large-area device ($D=2.5$ μm) made in the same processing run as some nm devices. The asymmetry of the two barriers is reflected in the asymmetry of the I-V curve with respect to the bias polarity.[27,28] The ratio of the peak current in positive and negative biases is 1:3.2. The current-threshold voltage in the negative bias $V_{\rm th}^{(-)}\approx1.3V_{\rm th}^{(+)}$ because of the different barrier thicknesses. The current-peak voltage in the negative bias $V_{\rm th}^{(-)}\approx2.8V_{\rm th}^{(+)}$ mostly because of the space charge of electrons accumulating in the well.[23] This device exhibits peak-to-valley current ratio of 54:1 in the positive and intrinsic bistability in the negative bias, indicating that our fabrication process does not lead to device quality degradation.

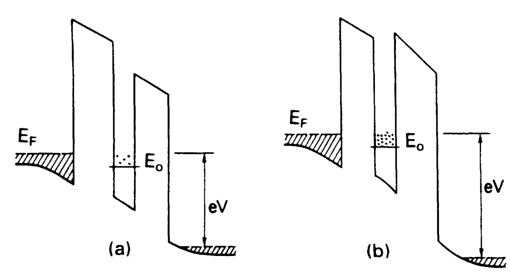

FIG. 1. Schematic energy diagrams of a large asymmetric DBRTS device under (a) positive and (b) negative bias. Hatching represents electron population of the emitter (left) and the collector (right) electrodes; dots represent the electron population in the well. E_0 is measured from the bottom of the well to the bottom of the subband of the 2D resonant states.

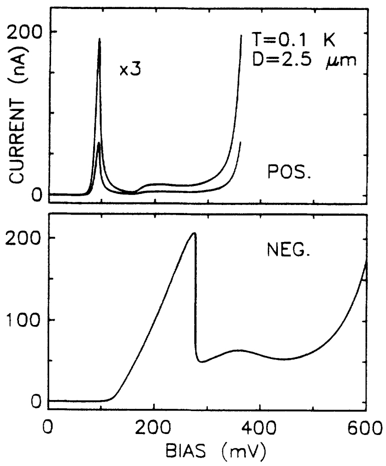

FIG. 2. *I-V* curve of a large-area device. The asymmetry of the *I-V* curve for positive/negative bias is due to the asymmetry of the barriers. Positive PTV ratio is 54.

IV. NANOMETER-SCALE DEVICES

A. Energetics

When the lateral size of a device is small, the energy spectrum of the states in the well is discrete because of the three-dimensional confining potential produced laterally by electrostatic depletion of the etched GaAs mesa walls and vertically by the two barriers. With application of bias, resonant tunneling is possible whenever the occupied states in the emitter are aligned with the well states as long as the charging effects are negligible. The density of states in the emitter electrode has been treated both as 3D (Refs. 5, 6, and 12) and as 1D.[1–3,13] The states in the emitter should be considered 1D or 3D depending on the relative magnitude of the size quantization in the emitter and the doping-induced broadening of these ideally 1D states (at low T). Thus the emitter is believed to be 3D-like in relatively large devices ($D \sim 500$ nm) and nearly 1D-like in smaller, pinched-off devices ($D \sim 150$ nm).

The lateral confining potential in the well of a DBRTS device has been usually modeled as a 2D parabolic well, but also[5,6] as a 2D cylindrical square well. The parabolic potential is a realistic mean-field description of the depletion potential for pinched-off or nearly pinched-off doped cylindrical electrodes; the square-well potential should model well relatively large devices, when there is a sizable undepleted core in the electrodes, where potential is flat. While more sophisticated models can be used in numerical simulations,[1] usually there is no qualitative difference in the results between them and the two simple models.

The infinite parabolic-well model is particularly simple mathematically, especially in magnetic field (Sec. V), but leads to accidental degeneracies of the well states which are often lifted in experimentally studied devices. For the devices of this paper, we employ the infinite parabolic-well model: the energies of the single-particle well states $Z_0\psi_{n,l}$ are $E_0+E_{n,l}$, where $E_{n,l}=(M+1)\hbar\omega_0$, with $M=(2n+|l|)$ and $(M+1)$-fold degeneracy; n and l are the quantum numbers, $n=0,1,2,\ldots$ and $l=0,\pm1,\pm2,\ldots$ (spin is ignored here). If the Coulomb interaction of the electrons in the well were turned off, the tunneling current would exhibit steplike, asymmetric peaks at biases such that $\Delta E=E_{n,l}$ with the step heights approximately proportional to $M+1$.[5,12,13]

However, tunneling of an electron into the well also involves a finite charging energy if the lateral size of the device is small. For cylindrical DBRTS devices, the charging energy $U_C=e^2/2C_W$, where the well effective capacitance[29] can be estimated simply as $C_W \approx \epsilon\epsilon_0\pi a^2/4d$ (for $a/d \gg 1$); it is determined by the device "electrical diameter" a,[30] effective barrier thickness d, and the material dielectric constant ϵ. The characteristic energy separation of the in-plane size quantization $\delta E=E_{n,l+1}-E_{n,l}=\hbar\omega_0 \approx 8\hbar^2/m^*a^2$ is determined by a and by the effective mass in the well m^*. The ratio $U_C/\delta E \approx de^2m^*/4\pi\epsilon\epsilon_0\hbar^2=d/a_B$, where $a_B \simeq 10$ nm is the GaAs effective Bohr radius; it is a independent. For typical $d=10$ nm, $U_C/\delta E \approx 1$. Thus the single-electron charging should be observable in DBRTS devices when size quantization is observed *and* $d/a_B \geq 1$.

B. Tunneling current

We proceed to consider the tunneling current for a nanometer-scale DBRTS device near V_{th}. At zero temperature, resonant-tunneling (RT) current of spin-polarized electrons tunneling from a 3D emitter through one state in the well is[6,12,13]

$$I^{(1)} \approx (e/\hbar)[T_E E_F T_C E_0/(T_E E_F + T_C E_0)] , \tag{1}$$

which assumes that coherence is lost while in the well and takes into account the Pauli principle for occupation of the well states. Equation (1) can be understood as follows.[23] Electrons near μ_E in the emitter tunnel into the well state. The average "attempt frequency" of tunneling electrons is $(\tau_E)^{-1} \approx T_E E_F/\hbar$. The current carried by one electron tunneling, on the average, every τ_E is e/τ_E. However, when the well state is already occupied by an electron, no other electron in the emitter can tunnel into the same well state because of the Pauli principle. Since an electron spends in the well, on the average, time $\tau_W \approx \hbar/T_C E_0$, the average tunneling rate is modified to $(\tau_E+\tau_W)^{-1}$. Multiplying this by e, we get $I^{(1)}$.

We discuss below dependence of I on ΔE, expressing ΔE in terms of single-particle energies $E_{n,l}$ in order to simplify the discussion. A more correct (but less quantitative) discussion of the energetics is given in Sec. V in the context of magnetotunneling.

In a strongly asymmetric DBRTS device, for $T_E \ll T_C$, $I^{(1)}$ is limited by the emitter barrier. At V_{th} ($I=0$ for $V<V_{\text{th}}$), $\Delta E-U_{1e}=E_{0,0}$ in a nanometer-scale device, compared with $\Delta E=0$ for a large-area device (remember that ΔE increases when bias is increased). For $E_{0,0}<\Delta E-U_{1e}<E_{0,1}$, current is $2I^{(1)}$ since electrons of either spin can tunnel, and the well is occupied by one electron at a time and only for a small fraction

($\sim T_E/T_C$) of the time. At $\Delta E - U_{1e} = E_{0,1}$, the current will triple to $\approx 6I^{(1)}$, since now tunneling can proceed through the well states $E_{0,0}$, $E_{0,1}$ and $E_{0,-1}$, assuming that all three states have corresponding occupied states in the 3D emitter. In this situation (for $T_E \ll T_C$), as the bias rises, tunneling current increases reflecting the greater number of the well states available for RT, such that $E_{n,l} < \Delta E - U_{1e}$, the well being occupied only by one electron at a time. It is energetically possible to have two electrons in the well at the same time for $\Delta E > E_{0,0} + U_{1e} + U_{2e}$.[31] However, the probability of the two-electrons-in-the-well-at-a-time tunneling (per available well state $E_{n,l}$) is on the order of $T_E/T_C \ll 1$, and it contributes little to the total current as long as $I \ll e/\tau_W \approx eT_C E_0/\hbar$ or, equivalently, the number of the well states available for tunneling $(M+1)(M+2) \ll T_C E_0/T_E E_F$.

The physics is very different for $T_E \gg T_C$, when $I^{(1)}$ is limited by the collector barrier. $\Delta E - U_{1e} = E_{0,0}$ at $V_{\rm th}$, similar to the previous case. For $E_{0,0} < \Delta E - U_{1e} < E_{0,1}$, current is $I^{(1)}$, however, since the well is occupied by one electron at a time but it is occupied most of the time. Electrons of either spin can tunnel but only one electron can tunnel at any given time. The charging energy to have the second electron in the well is usually greater than U_{1e} because it involves electron-electron repulsion in the well;[6,21] we denote the second-electron charging energy as U_{2e}.[31] Thus the bias has to be increased until $\Delta E > E_{0,0} + U_{1e} + U_{2e}$ in order to have two electrons in the well at the same time and thus to increase the current to $\approx 2I^{(1)}$ through the two-electron spin-singlet channel and until $\Delta E > E_{0,1} + U_{1e} + U_{2e}$ for the spin-triplet channel to become available. This topic is discussed further in Sec. V, in the context of magnetotunneling. In this situation ($T_E \gg T_C$), as the bias rises, tunneling current increases in steps, reflecting the increasing number of electrons in the well.

It should be noted that $I^{(1)}$ is not a constant even for a given device: it depends on V and B, for example, through T_E and T_C. Further, Eq. (1) gives the tunneling current only through the direct (energy- and lateral-angular-momentum-conserving) channel. However, in general, $I^{(1)}$ may depend on the dimensionality of the emitter states and on coupling of various emitter states with the well state, which may depend on the presence of ionized impurities, phonon modes, and interface roughness.[32,33]

C. Experimental data and discussion

Figure 3 shows I-V curves of a nanometer-scale device fabricated from the same wafer (Sec. II). The I-V characteristic has a peak current $I_P \approx 40$ pA in the positive and $I_P \approx 470$ pA in the negative bias. The tunneling current is immeasurably small (<0.1 pA) in both polarities as voltage is increased from zero to $V_{\rm th}$. Then current rises sharply at $V_{\rm th}$ and stays nearly constant in some bias range in both bias polarities, thus forming a step. The short-period (~ 1 mV) modulation is quite reproducible and shifts regularly with magnetic field (Sec. V), its origin is not fully understood at present.[34] Similar short-period modulation has been observed in all small devices and is somewhat more pronounced in the negative than in the positive bias.

The Coulomb blockade impedes tunneling until the first current step in both bias polarities. In the positive bias, the emitter barrier is less transparent, every well state through which tunneling is energetically allowed is occupied only for a small fraction of time. Thus, after overcoming the Coulomb blockade, tunneling can proceed through several well states even when there is at most only one electron in the well at any given time. As bias is increased, the current can increase reflecting the greater number of the well states available for the one-electron-at-a-time RT until it is energetically possible to have two electrons in the well at the same time. Even when it is energetically possible to have two electrons in the well at the same time, the two-electrons-at-a-time contribution to the current is small for ΔE less than $E_{1,1}$

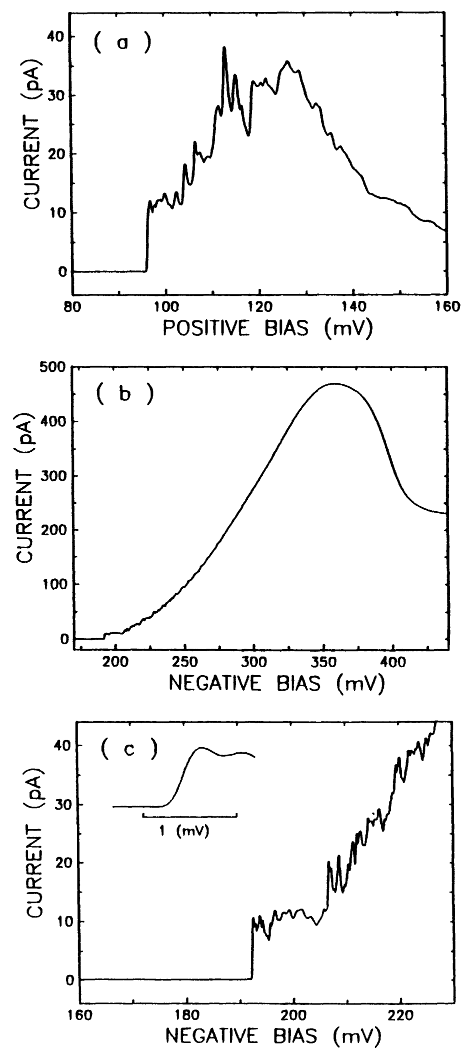

FIG. 3. I-V curves of a nanometer-scale DBRTS device at 20 mK for positive bias (a), and negative bias, (b) and (c). (c) is an enlargement of (b) near threshold; the first current step is magnified in the inset.

or $E_{1,2}$. We obtain $\hbar\omega_0 \approx 4$ meV from the magnetotunneling data (Sec. V). Thus we estimate that the I-V curve of Fig. 3(a) reflects the one-electron-at-a-time tunneling through an increasing number of size-quantized well states (degeneracy is largely lifted, as discussed in Sec. V) at least until $V = 130$ mV.

In the negative bias, the collector barrier is less transparent and, after overcoming the Coulomb blockade, the lowest well state is occupied most of the time. In contrast to the positive bias, even though the only tunneling electron can tunnel through several of the lowest well states, after the first current step the current stays nearly constant until it is energetically possible to have two electrons in the well at the same time, when the second step occurs. From the voltage extent of the first current step we estimate $U_{2e} \approx 4$ meV. Similarly, each subsequent current step occurs when it is energetically possible to have one more electron in the well. Thus the I-V curve of Fig. 3(b) reflects single-electron charging of the well by an incrementally increasing number of electrons dynamically stored in the well.

Figure 4 gives the derivatives of the negative-bias I-V curves for $B = 0$ and 7.5 T. The derivatives dI/dV were calculated numerically; an enlargement of the $B = 0$ derivative for $260 \le V \le 300$ mV is shown in the inset. One can clearly see the differential conductance peaks associated with the current steps in the I-V curves. In the $B = 0$ data, 33 peaks can be identified which correspond to 1 to 33 electrons dynamically stored in the well. The first three or four peaks are more clear in the $B = 7.5$ T data because the short-period modulation is suppressed by B. The Fourier transform reveals the quasiperiodicity of the $B = 0$ peaks for $240 < V < 320$ mV, corresponding to $8 \le N_W \le 27$, in Fig. 4. The quasiperiod in voltage is about 4.4 mV for $8 \le N_W \le 16$, it decreases to 3.6 mV for $17 \le N_W \le 27$; these correspond to the energies of 1.2 and 1.0 meV, respectively, using the bias-to-energy conversion coefficient $e\alpha^{(-)} = 0.28$ meV/mV (Sec. VI). These energies are interpreted as close to the values of U_C, the single-electron charging energy, for the ranges given. Indeed, the value of $U_C \approx 2.5$ meV near V_{th}, estimated from the device geometry, is expected to decrease as V rises because an increase in N_W leads to occupation of excited well states with greater spatial extent of the wave functions ("electrical size" increases with N_W). The quasiperiodic conductance peaks are observed in the negative-bias range where there are more than ~ 10 electrons in the well, while for $N_W < 4$ there is no quasiperiodicity whatsoever, as expected.

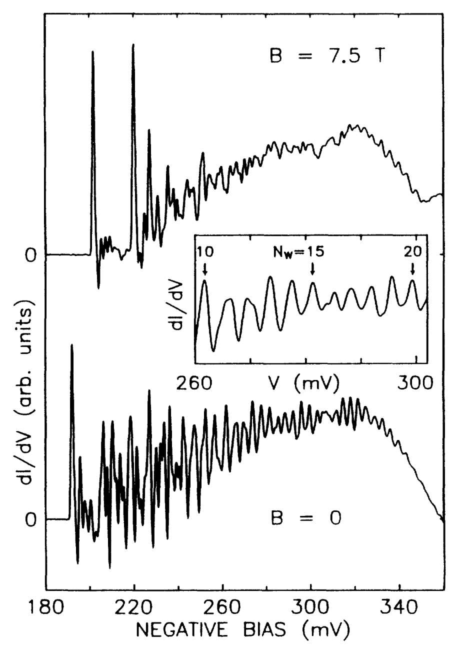

FIG. 4. Differential conductance calculated from the I-V curve shown in Fig. 3(b) ($B = 0$) and at $B = 7.5$ T. The short-period modulation (Ref. 34) obscures the peaks corresponding to current steps for $V < 250$ mV in the $B = 0$ data. Up to 33 peaks can be identified corresponding to one-by-one, starting from zero, addition of up to $N_W = 33$ electrons into the well. Inset gives an enlargement of the $B = 0$ data for $10 \le N_W \le 20$.

Figure 5 shows I-V curves in the negative bias of several devices made from the same heterostructure wafer. I_P gives a rough measure of the "electrical size" of a device.[5] Even though the values of I_P are quite different, the height of the first current step is nearly the same. Such uniformity of the values of $I^{(1)}$ is direct evidence for general validity of Eq. (1) and also for submonolayer control of the barrier layer thickness (≈ 10 nm, averaged laterally over $a^2 \sim 100 \times 100$ nm^2) within the distance between the devices of 1 mm. Also, the presence of a single donor in the central region of the well would considerably affect experimental I-V curves; many of our devices provide evidence for this, similar to that of Dellow *et al.*[4] Absence of such behavior, however, indicates that no donor occurs within a volume of $a^2 w \approx 1 \times 10^{-16}$ cm^3, giving residual donor density in the well as $\sim 5 \times 10^{15}$ cm^{-3}.

The calculated values of $2I^{(1)+} \approx 8$ pA and $I^{(1)-} \approx 11$ pA in the positive and negative polarity, respectively.

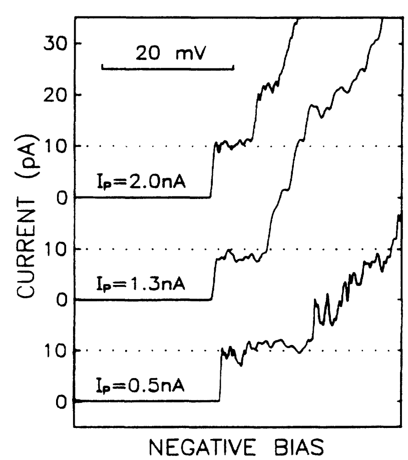

FIG. 5. I-V curves of several devices made from the same DBRTS wafer. I_P gives the peak current; it is a measure of the "electrical size" of a device at V_P (Ref. 30). The first current step height $I^{(1)}$ is independent of I_P.

The experimental values, obtained from the first current steps of several devices (Figs. 3 and 5, Ref. 6 and other nanodevices), are $2I^{(1)+}=9\pm2$ pA and $I^{(1)-}=9.5\pm1$ pA; the factor of 2 in the positive bias accounts for the spin degeneracy of the $E_{0,0}$ state. The agreement between the experimental and calculated values is very good because the transmission coefficients and other DBRTS parameters were obtained by fitting the data of a large-area device. Moreover, in the negative bias $T_E \gg T_C$ and we can estimate $I^{(1)-}$ as simply the current due to one electron tunneling every τ_W: $I^{(1)-}\approx 14$ pA, which is also in good agreement with experiment.

Several other observations are in order concerning the *I-V* curves of nanometer devices as compared to large-area devices: (i) V_{th} is pushed up to a higher (in magnitude) voltage; (ii) the peak-to-valley current ratio in the positive bias (~ 7) is considerably smaller than that of large-area devices ($>50{:}1$); (iii) the intrinsic bistability in the negative bias disappears as D is reduced below ~ 1 μm; (iv) the ratio of the peak currents in the positive and negative polarities is a factor of 3 greater in nm devices.

The shift of V_{th} to higher (in magnitude) voltage can be accounted for, in part, by the Coulomb blockade and by the $E_{0,0}$ upward shift of the lowest well state, relative to E_0, and, in part, in nearly pinched-off devices, by the greater penetration of the depletion field into the well[1,13] since the double-barrier region is doped weaker than the electrodes. The decrease of the peak-to-valley ratio in the positive bias in small-area devices is likely to originate in the Heisenberg uncertainty principle.[5,12] The uncertainty in the in-plane momentum of a tunneling electron is $\sim\hbar/a$, where a is the "electrical diameter" of the device. Thus conservation of the in-plane component of the momentum, violation of which by scattering gives rise to the valley current in large devices,[32] is replaced with the conservation of the in-plane angular momentum in nm devices. However, there are well states with small angular momentum, like $E_{n,0}$ or $E_{n,\pm1}$, at high energies $E_{n,l}>E_F$; RT through such states is therefore allowed even for $V>V_P$, in the valley region. Additional valley current also leads to a less steep fall of the I vs ΔE dependence in the NDR region, thus removing the bistability in the *I-V* curve.[23] The change in the ratio of the peak currents (iv) is not fully understood at present.

V. MAGNETOTUNNELING

Magnetic field has been used extensively as a powerful tool in experimental studies of quantum dots.[1–11,35] In this section, we report a magnetotunneling study of the same nanometer-scale DBRTS device. The asymmetry of the barriers enables us to largely separate the size-quantization and the single-electron charging effects in magnetic field also. The magnetic-field dependencies of the single-particle energies and the few-electron Coulomb interaction thus can be studied experimentally.

Figure 6 shows representative *I-V* curves with magnetic field B applied parallel to the tunneling direction ($B \parallel I$). We observe very different response to B of the *I-V* curves in the two bias polarities. As discussed in the preceding section, at zero field the first current step in both bias polarities occurs when the Coulomb blockade (U_{1e}) and the barrier for RT ($E_0+E_{0,0}$) are overcome. The current peaks in the positive polarity correspond to additional well states becoming available for RT, as bias is increased, such that $E_{n,l}<\Delta E(V)-U_{1e}$, the well being occupied only by at most one electron at a time. An *I-V* curve in this polarity thus reveals the size quantization of the well states. The *steplike* increase of current (Coulomb staircase) in the negative bias corresponds to the increase

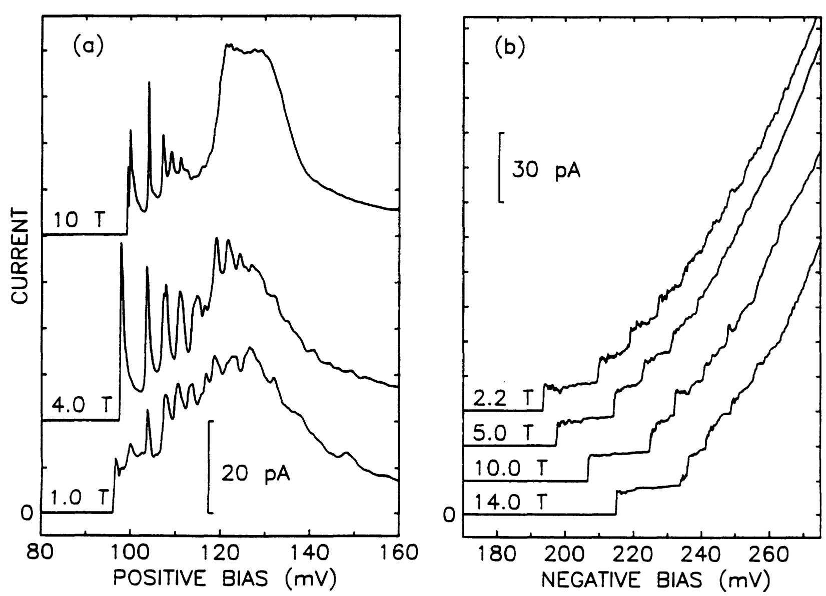

FIG. 6. Representative magnetotunneling data at 20 mK (B perpendicular to the barriers). Note the striking difference in the character of the data (peaks vs steps) in the two bias polarities.

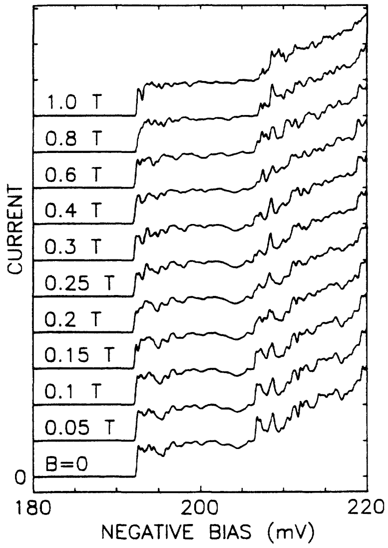

FIG. 7. Evolution of the short-period modulation at low magnetic fields. The curves are offset vertically by 12 pA.

of the number of electrons dynamically stored in the well. An I-V curve in this polarity thus reveals the incremental single-electron charging of the well. Figure 7 gives the I-V curves for several low B, focusing on the short-period (~ 1 mV) modulation, which shifts regularly with B.[34]

Figure 8 gives the I-V curves versus B data with B incremented by 0.3 T. Two different B dependences of the I-V curves in the two bias polarities reflect the different B dependences of the single-particle kinetic energies of the well states and the single-electron charging energies. In the positive bias, the first current step develops into a current peak at higher B. In this polarity, at higher bias, positions of the peaks (V_P) shift and cross systematically with rising B. Because of the Landau quantization in the emitter, E_F in the emitter oscillates with B. In order to avoid the complication from the B dependence of E_F in the emitter, we subtract V_{th} from V_P at each B. Figure 9 shows $V_P - V_{\text{th}}$ as a function of B. Since μ_E is aligned with the lowest well state at V_{th}, the $V_P - V_{\text{th}}$ vs B plot traces the B dependence of the well state energies with respect to the lowest one. It should be noted that this

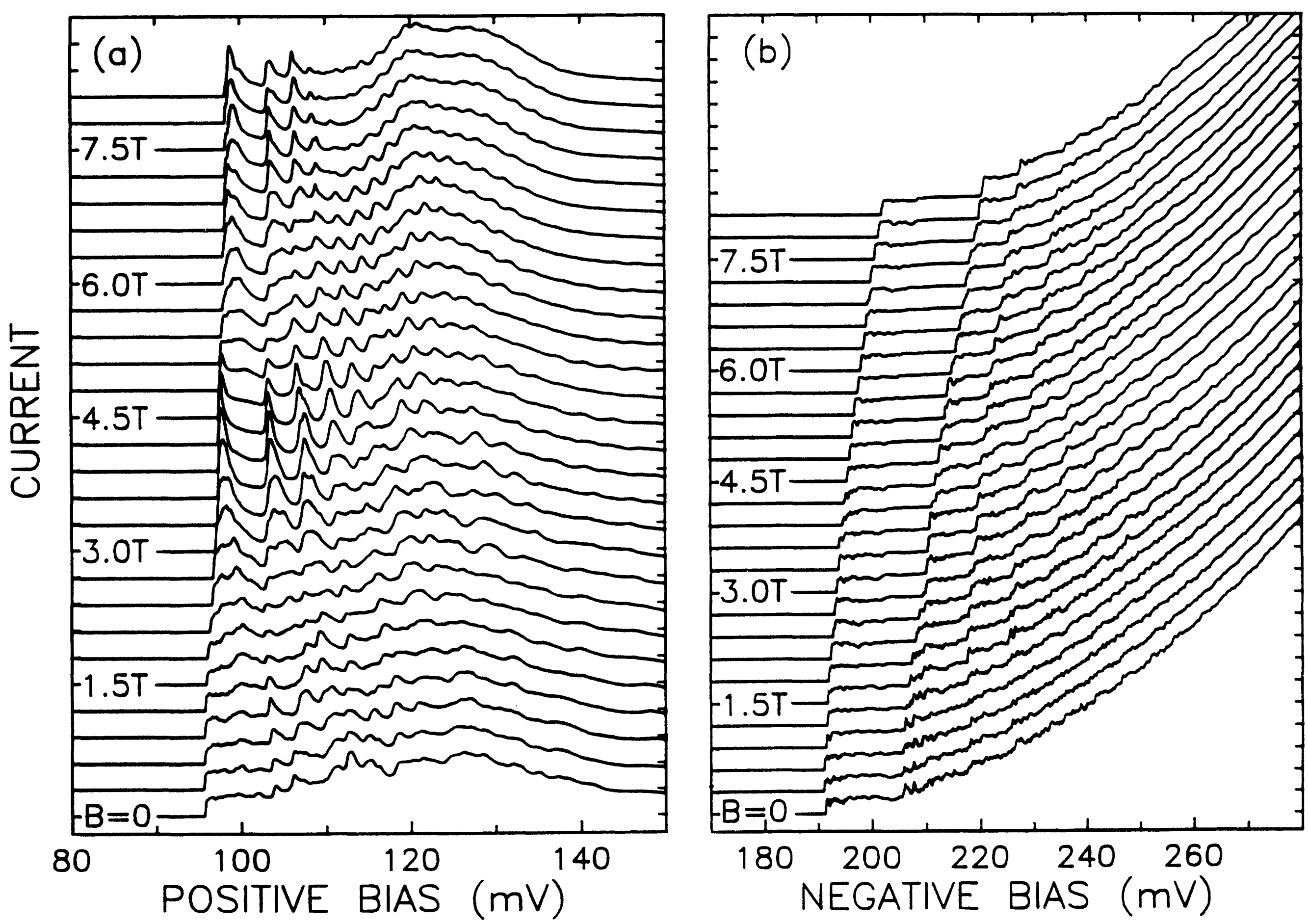

FIG. 8. Magnetotunneling data at 20 mK; curves shown were taken every 0.3 T and are offset vertically by 15 pA. There is at most one electron tunneling at a time in the positive bias; current peaks when a single-particle state in the well resonates with μ_E in the emitter. In the negative bias, each current step corresponds to increase by one in the number of electrons in the well ($N_W = 0$ at low bias). The shift of the first current step to higher bias is due, in part, to the $1/2\hbar\omega_c$ diamagnetic shift of the lowest well state, and, in part, to an in-plane component of slightly misaligned B.

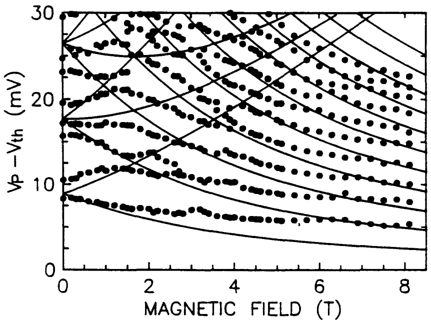

FIG. 9. Positions of experimental current peaks (relative to V_{th}) vs B in the positive bias (dots). Solid lines give the single-particle energies $E_{n,l}(B)-E_{0,0}(B)$, calculated for a parabolic confining potential with Eq. (2) using $\hbar\omega_0=4.0$ meV. $\hbar\omega_0$ is the only fitting parameter. Bias-to-energy conversion $e\alpha^{(+)}\approx 0.46$ meV/mV.

procedure removes (at every B) U_{1e} of the lowest well state from the energies of the excited well states; however, the first-electron charging energy U_{1e} should be somewhat smaller for the excited states because of the greater lateral extent of the electronic wave function in higher states. The data of Fig. 9 are qualitatively similar to the normal Zeeman splitting of electronic states in atoms.

In the negative bias, current steps (Coulomb staircase) become less obscured because the short-period modulation is, generally, suppressed by magnetic field. Up to six or seven steps can be seen in Fig. 8(b). We define ΔV_N as the voltage extent of the Nth current step in the negative bias, corresponding to the number of electrons in the well equal to N_W most of the time, and fluctuating to N_W-1 for the fraction of time on the order of $T_C/T_E \ll 1$. Figure 10 shows ΔV_N as a function of B for $N_W \leq 5$. At $B \to 0$, the first current step width is greater than the others, $\Delta V_1 > \Delta V_2 > \Delta V_3 \approx \Delta V_4 \approx \Delta V_5$. For $B > 3$ T, ΔV_1 increases somewhat with B, while the $N_W \geq 2$ step widths cluster together around $\Delta V \approx 7.5\pm 1$ mV in the experimental field range.

An analytical calculation of the single-particle energy spectrum in magnetic field can be done for a parabolic confining potential with rotational symmetry.[36] Electron energies (neglecting spin) are described by two quantum numbers (n,l):

$$E_{n,l}=(n+\tfrac{1}{2}+|l|/2)\hbar(\omega_c^2+4\omega_0^2)^{1/2}+(l/2)\hbar\omega_c\ , \qquad (2)$$

where ω_c is the cyclotron frequency and $\hbar\omega_0$ is the energy spacing of the parabolic potential at $\omega_c=0$. For $B=0$, Eq. (2) reduces to $E_{n,l}=(M+1)\hbar\omega_0$, with $M=2n+|l|$ and $(M+1)$-fold degeneracy for each spin. Magnetic field lifts this $(M+1)$-fold degeneracy. For $\hbar\omega_0=0$ (no confining potential), Eq. (2) reduces to $E_{n,l}=(N+\frac{1}{2})\hbar\omega_c$, with $N=n+l/2+|l|/2$, where N is the Landau-level index and l is the angular-momentum quantum number. In the high-field limit $\omega_c \gg \omega_0$, the energies of the negative l states are independent of l if $\omega_0=0$, but they are not degenerate and increase with $|l|$ in the presence of confining potential; the negative l states approach nth Landau level and the positive l states approach $(n+l)$th Landau level.

For comparison with experiment, we calculated the energies of the well states $E_{n,l}(B)$ using Eq. (2) with $\hbar\omega_0=4.0$ meV. The energies $E_{n,l}(B)-E_{0,0}(B)$ for several lowest well states were converted to voltages with the bias-to-energy conversion coefficient $\alpha=0.46$, as determined from the temperature dependence of the data (Sec. VI). The result (interpreted as theoretical V_P-V_{th}) is given by solid lines in Fig. 9. $\hbar\omega_0$ is used as the only fitting parameter; the value $\hbar\omega_0=4.0$ meV gives the most reasonable fit. Neither variation of U_{1e} in different well states, nor the likely nonparabolicity of the real confining potential, are reflected in the calculated solid lines. Agreement between the simple model calculation and the experimental data is qualitatively good. Numerical calculations[37] suggest that the qualitative behavior of the energies of the well states in magnetic field is insensitive to the exact shape of the confining potential.

Two interesting features are worth noting in Fig. 9. First, at high field, the data points follow curved lines rather nicely, similar to the calculated lines approaching the first Landau level. However, there are no data points that follow the calculated lines approaching the second Landau level, while in the low-field region ($B<2$ T) there are several branches of data points going up with B. This behavior is likely due to the conservation of the in-plane angular momentum (equivalently, conservation of Landau-level index) for tunneling from the emitter into the well. When B is high enough, all electrons in the emitter are in the lowest Landau level. These electrons can tunnel only into those well states that approach the first Landau level at high field. Second, the $B=0$ degeneracy of calculated well states is lifted in real devices (Fig. 9). The zero-field degeneracies arise from (i) the assumed infinite parabolic lateral confining potential and (ii) the assumed inversion symmetry of the vertical confining and crystal potentials. The first kind of degeneracies (e.g., $E_{1,0}=E_{0,\pm 2}$) are lifted if the lateral confining potential in the real device is not exactly parabolic and also because of the mixing of $E_{n,l}$ by the charging energy. However, the lifting of the l degeneracies (e.g., $E_{0,+1}=E_{0,-1}$) requires inversion asymmetry in the vertical direction. The symmetry under inversion can be removed via the spin-orbit coupling either by the microscopic crystal potential (GaAs lacks inversion symmetry) or by an external or built-in electric field.[38] Thus the lack of inversion symmetry of the vertical confining potential under applied bias offers us the most likely cause of the observed lifting of the zero-field l degeneracy.

The measurement of the width of the current steps as a function of B in the negative bias (Fig. 10) is, to our knowledge, the first experiment to directly investigate the electron-electron interaction in a quantum dot for just two to five electrons. Several theoretical investigations into this issue have been reported.[19–22,37,39] As discussed in Sec. IV, each step in the "staircase" corresponds to increase of N_W by one, starting from zero. A step width ΔV_N thus corresponds (so long as electrons tunnel from near μ_E in the emitter) to the total energy $\delta E_N+U_{(N+1)e}$ required for adding one more electron from μ_E into the well, changing from N_W to N_W+1 electrons.

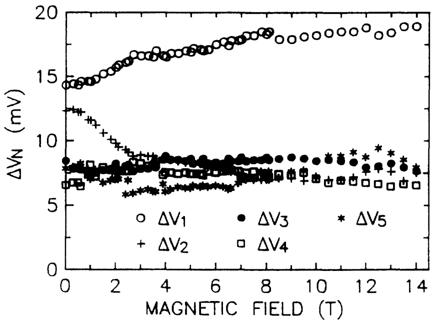

FIG. 10. The voltage extent of current steps ΔV_N, corresponding to charging of the well from N_W to N_W+1 electrons, as a function of B in the negative bias for the first five steps. Bias-to-energy conversion $e\alpha^{(-)} \approx 0.27$ meV/mV.

Here, δE_N gives the required kinetic energy: $\delta E_N \approx (E_{N+1}-E_N)/N_W$, where E_N are the kinetic energies of the many-body ground states (note that a many-electron ground state E_N is not an integer multiple of $\hbar\omega_0$), and $U_{(N+1)e}$ is the difference of the corresponding many-electron Coulomb energies, per electron, both charging and intrawell. At $B=0$, in a 2D parabolic potential, for large N_W, $E_N \approx (N_W)^{3/2}\hbar\omega_0$ and therefore δE_N typically fluctuates close to $\hbar\omega_0/(N_W)^{1/2}$. In the high-$B$ limit, for large but finite N_W, $\delta E_N \rightarrow 0$. At any B, for large but finite N_W, $U_{Ne} \rightarrow U_C$, a nearly (but not exactly[8]) constant value for a range of $\delta N_W \sim (N_W)^{1/2}$ (Sec. IV C).

The first width, ΔV_1, gives the energy difference between having just one and having two electrons in the well. As expected, ΔV_1 is greater than other ΔV_N because the Coulomb repulsion per electron is greatest for two electrons in the well. However, in experimentally studied devices, there are two complications usually not considered theoretically. First, at any B, U_{Ne} depends on the lateral extent a of the wave functions of the well-confined electrons; since a increases with N_W, U_{Ne} decreases as N_W is increased. Also, a high B reduces a somewhat; therefore, as $B \rightarrow \infty$, U_{Ne} is expected to increase (this effect is particularly important for small N_W). Second, screening by the electrodes reduces the intrawell Coulomb repulsion. For electron density in the electrodes $n_E = 2\times10^{17}$ cm^{-3}, the screening length is $n_E^{1/3} \approx 15$ nm. This length is in addition to the barrier thickness of about 10 nm so that screening charges in the electrodes are $\lambda \approx 25$ nm away from the electrons in the well. The in-plane separation of the electrons in the well is on the order of $a/2 \approx (2\hbar/m^*\omega_0)^{1/2}$, on the average; for $\hbar\omega_0 = 4$ meV and $N_W=2$, $a/2 \approx 24$ nm. Thus the separation of electrons in the well and the distance to the screening charges are comparable. An estimate of the expectation value of the two-electron intrawell repulsion energy, cut off for electron separations greater than λ,

$$\int_{|\mathbf{r}_{12}|<\lambda} (e^2/4\pi\epsilon\epsilon_0|\mathbf{r}_{12}|)|\psi(\mathbf{r}_1,\mathbf{r}_2)|^2 d\mathbf{r}_1 d\mathbf{r}_2 \,,$$

shows that the screening reduces the bare repulsion by a factor of 2 ± 0.5 (for $N_W=2$) for the parameters of this device.

There are two possible two-electron states; spin singlet and spin triplet. At zero B, the singlet state has lower energy than the triplet state; at some B, the $S_Z=-1$ triplet state crosses the singlet state. Experimentally, we observe evidence for splitting of the second current step into two substeps in the I-V curve in the negative bias [with more or less clarity for different devices, Fig. 8(b) and Ref. 6]. The crossing of the $S_z=-1$ triplet state and the singlet state occurs at $B \approx 3$ T; this value of B yields the exchange-enhanced value of $g^* \approx 7$. The crossing is reflected as cusps in ΔV_1 and ΔV_2 at the same $B \approx 3$ T in Fig. 10: upward cusp in ΔV_1 and downward cusp in ΔV_2. All other step widths ($N_W > 2$) cluster together, particularly for $B > 1$ T (Fig. 10). This indicates that $U_{(N+1)e} + \delta E_N$, the energy required for adding one more electron into the well, is only weakly sensitive to the number of electrons in the well provided there are already two or three electrons there.

VI. TEMPERATURE DEPENDENCE

In this section, we report on our study of the temperature dependence of the I-V curves of the nanometer-scale DBRTS device of Fig. 3. We are able to fit satisfactorily the first current step in the I-V curves in both bias polarities by the Fermi-Dirac (FD) distribution function. Figure 11 shows the I-V curves near the threshold $V_{\rm th}$ at several temperatures T. The structure in both bias polarities is smoothed as T increases; most of the structure in the I-V curves washes out by 15 K. Note that the short-period modulation,[34] superimposed on current steps in both bias polarities, is quite reproducible and smooths out at roughly the same T as the steps and the peaks. This indicates that all structure in I-V curves originates in the same tunneling process.

When T is raised, the electron distribution at μ_E in the emitter smears according to the FD distribution function. Thermally excited electrons in the emitter can tunnel into the well when the energy difference between μ_E and the well states, including the charging energy, is $\sim kT$. The steps and peaks in the I-V curves are expected to be smoothed at finite T and eventually to be washed out at T such that $\sim 5kT$ is equal to the characteristic energies of the device (δE and U_c).[15-18] Values of $U_C \sim 25$ K and $\delta E \approx 50$ K, obtained from the voltage extent of the current steps in the negative bias and from the fitting of current peaks in the positive bias (Sec. V), are consistent with the observed T dependence of Fig. 11.

For the rest of this section we will focus on the first current steps (FCS) in both bias polarities, which correspond to at most one electron in the well at a time. Figure 12 gives the expanded FCS in the positive and negative bias at different temperatures.[40] It is necessary to distinguish between the bath temperature T and the effective electron temperature in the emitter $T_{\rm eff}$, especially at low T. $T_{\rm eff} \geq T$ because of the Joule heating of the device and/or injection of hot electrons into emitter. We measure T directly, but $T_{\rm eff}$ has to be extracted from the I-V data and, in general, cannot be assumed to equal

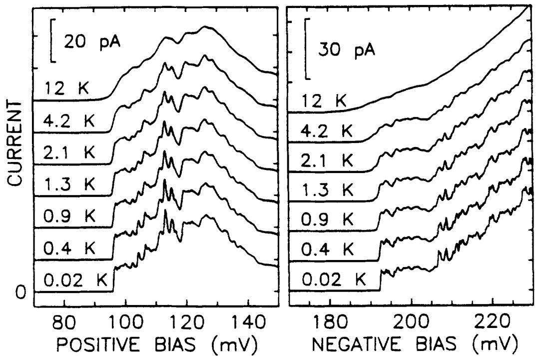

FIG. 11. The temperature evolution of the I-V curves.

T. We fit the experimental I-V curves for a FCS at various T by the FD function as

$$I(V)=I_0/\{1+\exp[-\alpha e(V-V_{\mathrm{th}})/(kT_{\mathrm{eff}})]\}\ , \tag{3}$$

where I_0 is the FCS height and is taken to be T independent. The bias-to-energy conversion coefficient is defined theoretically as $\alpha e=d(\Delta E)/d(V)$, where e is the electronic charge. $\alpha<1$; it gives the fraction of the total bias corresponding to ΔE, the energy shift of the lowest well state relative to the emitter μ_E. Generally speaking, α is bias dependent; here, however, we are only interested in a small bias range around V_{th}, therefore we take α to be a constant. α can also be calculated for both polarities within a generalization of the self-consistent DBRTS model for large-area devices;[23] for the DBRTS of this paper we obtain $\alpha_{\mathrm{cal}}^{(+)}\approx0.45$ for the positive and $\alpha_{\mathrm{cal}}^{(-)}\approx0.28$ for the negative bias.

Equation (3) follows directly from the model where a DBRTS device is represented by a 3D Fermi sea in the emitter and one 3D-confined, discrete state in the well. In general, the tunneling current from the emitter through the well state is proportional to the convolution of the electron distribution in the emitter and the density of unoccupied states in the well, shifted upward in energy by U_{1e}. The electron distribution in the emitter is the product of density of states and the FD function. For a small energy interval near μ_E, we can approximate the density of states in the emitter as a constant. This is a good approximation as long as T is not too high, $kT\ll E_F$. The density of states in the 0D well is approximated by a δ function, since the lifetime broadening of the well state $\hbar/\tau_W\sim0.1\ \mu\mathrm{eV}\ll kT$. Energy conservation requires that only those electrons in the emitter can tunnel whose energy is aligned (at a given V) to the energy of the well state plus U_{1e}. Thus, in this model, when voltage is swept near V_{th}, the tunneling current directly gives the FD function.

The fitting of the data with Eq. (3) involves only one fitting parameter since $I(V)$ depends only on the ratio of T_{eff}/α. Figure 13 shows examples of the fitting for three T for each bias. It is apparent that FD function gives a very good fit to the measured FCS in the I-V curves; the fits are especially good in the tail (low V) region. From the fitting parameter obtained at every T, α is determined as follows. Since Eq. (3) depends only on the ratio T_{eff}/α, we plot this ratio versus the measured bath temperature T (not shown). For $T_{\mathrm{eff}}=T$, the plot should follow a straight line and the slope gives the value of α. Indeed, we see a linear relation in the T_{eff}/α vs T plot in certain temperature range. From the slope of this plot we determined α_{exp} for each bias polarity: $\alpha_{\mathrm{exp}}^{(+)}=0.46\pm0.04$ and $\alpha_{\mathrm{exp}}^{(-)}=0.27\pm0.03$. These values are very close to those obtained from the self-consistent model calculation. However, at low temperatures ($T<300$ mK) and at high temperatures ($T>4$ K), we ob-

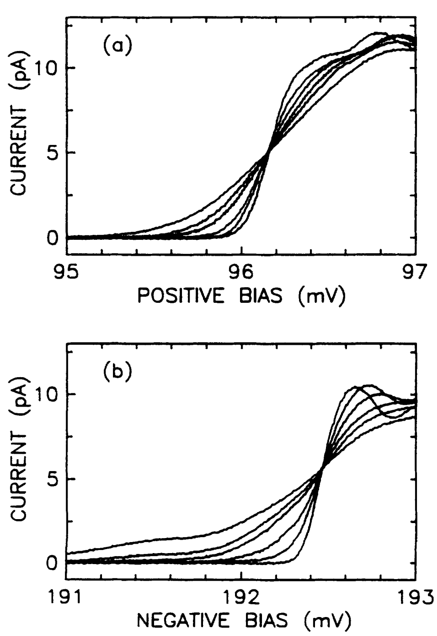

FIG. 12. Expanded plot of the temperature evolution of the first current step. The temperatures are 20 mK (the sharpest), 220 mK, 430 mK, 0.69 K, 0.92 K, and 1.3 K (the smoothest).

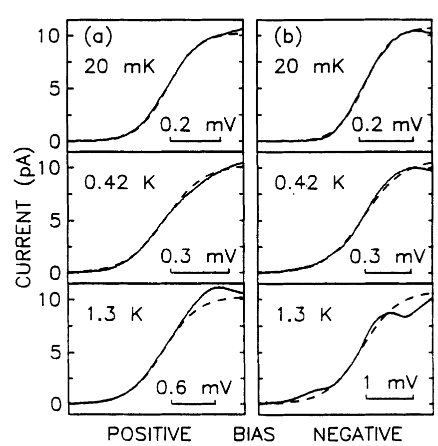

FIG. 13. First current steps of the experimental I-V curves (solid lines) fitted by the corresponding Fermi-Dirac distribution function (dashed lines).

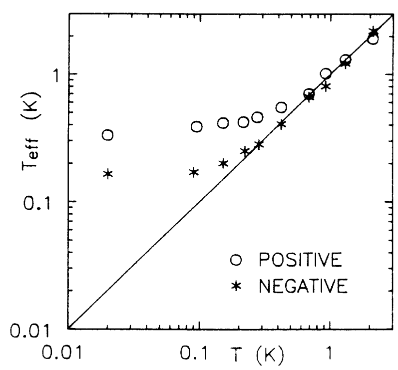

FIG. 14. Effective temperature T_{eff}, obtained by fitting I-V data with Eq. (3), vs the measured bath temperature T. The deviation from the expected equality $T_{\text{eff}}=T$ at low $T<300$ mK is explained by electrical pickup rather than by electron heating. Uncertainties in T_{eff} are typically 10%.

serve deviation from this linear relation. The high-T deviation is expected because then thermally excited electrons can tunnel through the excited well states not included in the model of the density of well states as a single δ function. Also, the density of states in the emitter can no longer be approximated as a constant for $\sim 4kT > 2$ meV.

The deviation from linearity at low T is interpreted as saturation of the effective temperature T_{eff} at a finite value as $T\rightarrow 0$. We plot T_{eff} vs T in Fig. 14. T_{eff} approaches 340 mK in the positive and 170 mK in the negative bias as $T\rightarrow 0$. There are two possible causes for the saturation of T_{eff} at low T. First, the electronic temperature in the emitter differs from the lattice temperature because of the Joule heating of the electron system by, for example, the flowing dc current I and/or ac noise current. The Joule heating by dc and shot-noise currents are proportional to the tunneling current (or I^2), both are negligible for $I<10$ pA (at lowest T, Joule heating is expected to become nonnegligible for $I>100$ pA). The estimated heating power due to the Johnson and pickup noise currents is also many orders of magnitude too small to cause such deviation at low T.[41] Heating cannot account for the different limiting values of T_{eff} as $T\rightarrow 0$ in the two polarities.

Second, T_{eff}, determined as described above, has contributions not only from the effective electron temperature, but also from any ac voltage, which, applied to the device, averages the "true" dc I-V curves. For example, electromagnetic pickup by the measuring circuit, superimposed on the dc bias, produces averaging ac voltage. We assume that the electrical pickup has a Gaussian distribution, namely, that the probability $P(V)$ for the instantaneous biasing voltage to have value V is

$$P(V)=[(2\pi)^{1/2}V_n]^{-1}\exp[-(V-V_{\text{dc}})^2/(2V_n^2)]\ ,$$

where V_{dc} is the applied dc bias and V_n is the variance of the Gaussian distribution. We fit FCS by this Gaussian-averaging voltage at the lowest $T=15$ mK since at this T the ac-voltage averaging dominates the temperature smoothing. Fitting yields $V_n\approx 100\pm 10$ μV for both bias polarities. The different saturation values of T_{eff} in the two polarities are thus explained by our translating the voltage averaging into the energy averaging through different coefficients α.

ACKNOWLEDGMENTS

We are grateful to M. Shayegan for heterostructure material used in initial stages of this work,[5] to J. E. Lukens for use of electron-beam lithography facility, and to J. K. Jain, D. V. Averin, G. W. Bryant, L. Eaves, N. F. Johnson, M. A. Kastner, R. W. Landauer, C. S. Lent, K. K. Likharev, H. C. Liu, M. A. Read, D. C. Tsui, and N. S. Wingreen for discussion of various aspects of nanometer RT and Coulomb blockade theory and experiment in the past four years. This work was supported in part by the Alfred P. Sloan Foundation and the NSF.

[1]M. A. Reed *et al.*, Phys. Rev. Lett. **60**, 535 (1988); Festkoerperprobleme **29**, 267 (1989).

[2]M. Tewordt *et al.*, J. Phys. Condens. Matter **2**, 8969 (1990); Appl. Phys. Lett. **59**, 1966 (1991).

[3]S. Tarucha, Y. Hirayama, T. Saku, and T. Kimura, Phys. Rev. B **41**, 5459 (1990); S. Tarucha and Y. Hirayama, Phys. Rev. B **43**, 9373 (1991).

[4]M. W. Dellow *et al.*, Electron. Lett. **27**, 134 (1991); in *Nanostructures and Mesoscopic Systems,* edited by W. P. Kirk and M. A. Reed (Academic, New York, 1991).

[5]B. Su, V. J. Goldman, M. Santos, and M. Shayegan, Appl. Phys. Lett. **58**, 747 (1991).

[6]V. J. Goldman, B. Su, and J. E. Cunningham, in *Nanostructures and Mesoscopic Systems,* edited by W. P. Kirk and M. A. Reed (Academic, New York, 1991).

[7]B. Su, V. J. Goldman, and J. E. Cunningham, Science **255**, 313 (1992).

[8]U. Meirav, M. A. Kastner, and S. J. Wind, Phys. Rev. Lett. **65**, 771 (1990); P. L. McEuen *et al.*, *ibid.* **66**, 1926 (1991).

[9]L. P. Kouwenhoven *et al.*, Z. Phys. B **85**, 367 (1991).

[10]D. C. Glatlli, C. Pasquier, U. Meriav, F. I. B. Williams, Y. Jin, and B. Etienne, Z. Phys. B **85**, 375 (1991).

[11]A. A. M. Staring *et al.*, Physica B **175**, 226 (1991).

[12]H. C. Liu and G. C. Aers, Solid State Commun. **67**, 1131 (1988); J. Appl. Phys. **65**, 4908 (1989).

[13]G. W. Bryant, Phys. Rev. B **39**, 3145 (1989); **44**, 12 837 (1991).

[14]H. van Houten, and C. W. J. Beenakker, Phys. Rev. Lett. **63**, 1893 (1989).

[15]A. N. Korotkov, D. V. Averin, and K. K. Likharev, Physica B **165-166**, 927 (1990); Phys. Rev. B **44**, 6199 (1991).

[16]Y. Meir, N. S. Wingreen, and P. A. Lee, Phys. Rev. Lett. **66**, 3048 (1991).

[17]A. Groshev, Phys. Rev. B **42**, 5895 (1990); A. Groshev, T. Ivanov, and V. Valtchinov, Phys. Rev. Lett. **66**, 1082 (1991).

[18]L. I. Glazman and R. I. Shekhter, J. Phys. Condens. Matter **1**, 5811 (1989); L. I. Glazman and K. A. Matveev, Pis'ma Zh. Eksp. Teor. Fiz. **98**, 870 (1990) [JETP Lett. **71**, 483 (1990)].

[19]L. Y. Chen and C. S. Ting, Phys. Rev. B **44**, 5916 (1991).

[20]N. F. Johnson and M. C. Payne, Phys. Rev. Lett. **67**, 1157 (1991); Phys. Rev. B **45**, 3819 (1992).

[21]G. W. Bryant, Phys. Rev. Lett. **59**, 1140 (1987).

[22]U. Merkt, J. Huser, and M. Wagner, Phys. Rev. B **43**, 7320 (1991).

[23]V. J. Goldman, D. C. Tsui, and J. E. Cunningham, Phys. Rev. B **35**, 9387 (1987); Phys. Rev. Lett. **58**, 1256 (1987).

[24]S. Luryi, Appl. Phys. Lett. **47**, 490 (1985).

[25]C. J. Gorter, Physica **17**, 777 (1951); I. Giaever and H. R. Zeller, Phys. Rev. Lett. **20**, 1504 (1968).

[26]T. A. Fulton and G. J. Dolan, Phys. Rev. Lett. **59**, 109 (1987); reviewed by D. V. Averin and K. K. Likharev, in *Mesoscopic Phenomena in Solids,* edited by B. L. Altshuler, P. A. Lee, and R. B. Webb (Elsevier, Amsterdam, 1991), p. 169.

[27]V. J. Goldman, D. C. Tsui, and J. E. Cunningham, Solid State Electron. **31**, 731 (1988); A. Zaslavsky, V. J. Goldman, D. C. Tsui, and J. E. Cunningham, Appl. Phys. Lett. **53**, 1408 (1988).

[28]Bias polarity is with respect to the substrate.

[29]While the semiclassical geometric capacitance does not describe the problem (Refs. 6, 19, and 20), an "effective capacitance" of the well to the outside world can be formally defined as $C_W = e^2/2U_{Ne}$; thus defined C_W depends, for example, on the shape of the confining potential, N_W, and B. We estimate $C_W \approx 3\times 10^{-17}$ F for $N_W = 1$ ($U_{1e} \approx 2.5$ meV) for the device of Fig. 3.

[30]For the larger device of Ref. 6, we determined $a \approx 120$ nm by fitting the size quantization and $a \approx 130$ nm by scaling the peak current density; for the device of Fig. 3, we obtain $a \approx 50$ nm (for $N_W = 1$) from the size quantization.

[31]U_{2e} is the *second*-electron charging energy, not the *two*-electron charging energy. That is, the first electron can tunnel into the well when $\Delta E^{(1)} = E_1 + U_{1e}$ (the kinetic energy of the in-plane motion of the one-electron ground state is E_1); the second electron can tunnel into the well when $\Delta E^{(2)} = (1/2E_2 - E_1 + U_{2e}) + \Delta E^{(1)} = 1/2E_2 + U_{1e} + U_{2e}$ (the kinetic energy of the two-electron ground state is E_2). In the limit $U_{Ne} \ll \delta E$ (for example, $\epsilon \rightarrow \infty$), the ground-state kinetic energies are integer multiples of $\hbar\omega_0$ (for example, $E_1 = E_{0,0}$). If $U_{Ne} \sim \delta E$, however, Coulomb interaction mixes the single-particle states even for $N_W = 1$; that is, the total N_W ground-state energy is minimized by an admixture of the higher single-particle states.

[32]V. J. Goldman, D. C. Tsui, and J. E. Cunningham, Phys. Rev. B **36**, 7635 (1987).

[33]Many contributions in *Resonant Tunneling in Semiconductors,* edited by L. L. Chang, E. E. Mendez, and C. Tejedor (Plenum, New York, 1991).

[34]The short-period modulation is superficially similar to the "universal" conductance fluctuations, but occurs in tunneling transport. Emitter electrode contains only $\sim n_E a^3 \approx 100$ donors in the volume from which electrons tunnel. Thus, the density of states in the emitter is modulated on the energy scale of $E_F/100 \approx 0.2$ meV giving rise to (0.2 meV)/$[e\alpha^{(-)}] \approx 0.8$ mV modulation of the tunneling current. As bias is raised, a greater number of donors (within the energy interval ΔE) contribute to the tunneling current and the influence of individual donors averages out.

[35]For example, W. Hansen *et al.*, Phys. Rev. Lett. **62**, 2168 (1989); C. Sikorski and U. Merkt, *ibid.* **62**, 2164 (1989); T. P. Smith III, Surf. Sci. **229**, 239 (1990).

[36]V. Fock, Z. Phys. **47**, 446 (1928); C. G. Darwin, Proc. Cambridge Philos. Soc. **27**, 86 (1930); R. B. Dingle, Proc. R. Soc. London Ser. A **211**, 500 (1952).

[37]C. S. Lent, Phys. Rev. B **43**, 4179 (1991); F. Geerinckx, F. M. Peeters, and J. T. Devreese, J. Appl. Phys. **68**, 3435 (1991).

[38]E. O. Kane, in *Handbook on Semiconductors* (North-Holland, New York, 1982), Vol. I, p. 193; J. P. Eisenstein, H. L. Stormer, V. Narayanamurti, A. C. Gossard, and W. Wiegmann, Phys. Rev. Lett. **53**, 2579 (1984); G. Lommer, F. Malcher, and U. Rossler, *ibid.* **60**, 728 (1988); R. Eppenga and M. F. H. Schuurmans, Phys. Rev. B **37**, 10923 (1988).

[39]P. A. Maksym and T. Chakraborty, Phys. Rev. Lett. **65**, 108 (1990); A. Kumar, S. E. Laux, and F. Stern, Phys. Rev. B **42**, 5166 (1990).

[40]An interesting feature is that a small bump emerges in the tail region of FCS as T increases in the negative bias. It can be clearly seen in the I-V curves at 1.3 and 2.1 K [Figs. 11(b) and 12]. We believe that this bump has the same origin as the short-period modulation (Ref. 34).

[41]In a similar experimental setup, electron temperatures as low as 15 mK were achieved in the fractional quantum Hall effect regime [V. J. Goldman, J. K. Jain, and M. Shayegan, Phys. Rev. Lett. **65**, 907 (1990)]. Thus we expect to achieve comparable electron temperatures in present samples.